

Metabolomic Analysis of Human Papillary Thyroid Carcinoma Using UPLC-Q-TOFMS

Guodong Man^{1,2}; Ruixia Ma³; Jianli Wang¹; Juan Wang¹; Qinjiang Liu¹; Jianye Zhou⁴; Jun Wang^{1*}

Abstract

Papillary thyroid carcinoma is the most common type of thyroid cancer worldwide, but its underlying mechanisms remain unclear. The aim of this study was to develop a non-targeted, metabolism-based tissue metabolomic analysis method to comprehensively identify the papillary thyroid carcinoma metabolic network with clinical samples. Ultra-high-performance liquid chromatography and quadrupole-time-of-flight mass spectrometry (UPLC-Q-TOFMS) was used to analyze metabolic changes in matched papillary thyroid carcinoma and paracancerous thyroid tissues obtained from patients. Principal component analysis, partial least square discriminant analysis, and orthogonal partial least square discriminant analysis models were used to separate paracancerous human thyroid and papillary thyroid carcinoma samples. In papillary thyroid carcinoma samples, the levels of L- α -amino acids, leucine, β -amino acids, valine, alanine, methionine, and their derivatives, as well as those of polypeptides, were significantly lower than those in paracancerous tissue. In contrast, the levels of dibucaine, propylamide, tyrosine, pidotimod, deoxysappanone B 7,4'-dimethyl ether, hippurate, and emodic acid were significantly increased in papillary thyroid carcinoma. In addition, metabolites with significant differences in expression were mainly involved in amino acid biosynthesis and metabolism and the mammalian target of rapamycin (mTOR) metabolic pathway. According to the results of our metabolomic and bioinformatic analyses, various metabolites may regulate the synthesis and expression of proteins in papillary thyroid carcinoma by regulating amino acid metabolism and mTOR-related pathways, which may be related to papillary thyroid carcinoma pathogenesis. This study provides novel insights into the metabolic abnormalities of papillary thyroid carcinoma and presents a potential method for its treatment.

Background

The incidence of thyroid cancer is increasing worldwide,¹⁰ and the disease ranked ninth among the most common cancers in women globally in 2020.²¹ Thyroid cancer contributes to over 586,000 cancer cases and 43,600 deaths each year.⁶ Papillary thyroid carcinoma (PTC) is the most common type of thyroid cancer, accounting for approximately 90% of all thyroid cancers, and mainly occurs in women aged 30–45 years. PTC shows good differentiation and a low degree of malignancy but is prone to lymph node metastasis in the early stages. Therefore, early diagnosis and timely treatment are important for

improving the survival duration of patients with PTC.^{16,3} However, ultrasound and ultrasound-guided fine needle aspiration biopsy have a specificity and negative prediction rate of 86.7% and 72.2%, respectively, for microcancer.²⁸ Consequently, patients are concerned about invasive examination methods. To improve the cure rate of patients with thyroid cancer, new screening methods are required to diagnose the disease more accurately and formulate new medical strategies for advanced thyroid cancer. Cancer has been suggested to be a metabolic disease.²⁴

¹ Gansu Provincial Cancer Hospital, Lanzhou, Gansu, China

² Gansu Provincial Academic Institute for Medical Research, Lanzhou, Gansu, China

³ The First School of Clinical Medicine, the First Hospital of Lanzhou University, Lanzhou University, Lanzhou, Gansu, China

⁴ Northwest Minzu University, Lanzhou, Gansu, China

Address correspondence to: Jun Wang, Gansu Provincial Cancer Hospital, Lanzhou, Gansu, China (jack3376@126.com)

Financial Disclosures: This work was supported by the Gansu Provincial Science and Technology Program Grant (Natural Science Foundation of Gansu Province), Project No: 22JR5RA646.

0024-7758 © Journal of Reproductive Medicine®, Inc.

The Journal of Reproductive Medicine®

Metabolomics based on nuclear magnetic resonance spectroscopy has been widely used to study thyroid cancer and, particularly, its diagnosis. However, the metabolic pathways driving PTC development remain unclear. Non-targeted metabolomic analysis is an efficient method combining multiparametric analysis methods. To improve thyroid cancer diagnostic accuracy, we aimed to develop a non-targeted metabolism-based tissue metabolomic analysis method to identify the comprehensive PTC metabolic network with clinical samples. We studied the overall metabolic characteristics of thyroid cancer tissues and identified sensitive and specific biomarkers for thyroid cancer diagnosis and progression. Our findings may improve thyroid cancer diagnostic accuracy and the treatment success rate.

MATERIALS AND METHODS

Sample collection

The ethics committee of the Gansu Provincial People's Hospital approved this study (approval number: P202205300031); all participants provided informed consent. Matched PTC (group C) and paracancerous thyroid tissues (group NC) were obtained from patients with PTC with the same diagnosis (nude 30; women; age 31–58 years; tumor size 0.2–3.6 cm). All patients underwent thyroid surgery at the Gansu Provincial People's Hospital. The pathological diagnosis of PTC was independently confirmed by two pathologists. The tumor samples were micro-dissected to ensure that more than 90% of the analyzed tissues contained cancer cells and that paracancerous tissues were not associated with follicular adenomas or thyroid cancers. None of the patients received radiotherapy or neoadjuvant chemotherapy before surgery. Fresh tumor and corresponding paracancerous thyroid tissues were rinsed with phosphate buffer after thyroidectomy, frozen with liquid nitrogen during the operation, and preserved at -80°C until analysis.

Instruments and chemicals

In this study, we used a mass spectrometer (TripleTOF 5600+ Mass Spectrometer; Sciex, Framingham, MA, USA), chromatography system

(Agilent 1290 Ultra-High Performance Liquid Chromatography System; Agilent Technologies, Santa Clara, CA, USA), and a chromatographic column (ACQUITY UPLC BEH Amide 1.7 μm , 2.1 mm \times 100 mm column; Waters Corporation, Milford, MA, USA). The chemicals used in this study were acetonitrile (1.00030.4008; Merck Millipore, Burlington, MA, USA), methanol (1.06007.4008; Merck Millipore), ammonium acetate (3594; Sigma-Aldrich, St. Louis, MO, USA), and ammonia water (105426; Merck, Darmstadt, Germany).

Sample preparation

Samples

Two groups of samples were tested, with 30 biological replicates per group. For quality control (QC), blank samples were prepared simultaneously. The QC samples were used to calibrate the gas chromatography and mass spectrometry (MS) system, determine instrument status, and evaluate system stability.

Metabolite extraction

The samples were ground in liquid nitrogen, and 100 mg of each sample was mixed with 200 μL of precooled water and 800 μL of precooled methanol/acetonitrile. Thereafter, the samples were precipitated via ultrasonication for 1 h on ice and incubated at 20°C for 1 h. Thereafter, the supernatant was centrifuged at $16,000 \times g$ for 20 min at 4°C . Subsequently, the supernatant was evaporated using a high-speed vacuum-concentration centrifuge system (Biofuge Stratos; Thermo Fisher Scientific, Waltham, MA, USA). For MS, the sample was re-dissolved in 100 μL of acetonitrile-aqueous solution and centrifuged at $16,000 \times g$ for 20 min at 4°C , and the supernatant was collected for analysis.

LC-MS/MS analysis

Chromatographic separation

Throughout the analytical process, the samples were placed in an automatic injector at 4°C . Sample separation was performed on an Agilent 1290 Infinity LC ultra-high performance liquid chromatography (UPLC) system and HILIC

column (5 μ L; Agilent Technologies) at a flow rate of 0.3 mL/min at 25 °C. Mobile phase A was water mixed with 25 mM ammonium acetate and 25 mM ammonia, whereas phase B was acetonitrile. The chromatographic gradient elution protocol was as follows: 0–0.5 min, 95% B; 0.5–7 min, 65%–95% B; 7–9 min, 40%–65% B; 9–10 min, 40% B; 10–11.1 min, 40%–95% B; 11.1–17 min, 95% B. The QC samples were inserted in the sample queue to monitor and evaluate system stability and experimental data reliability.^{11,14,12}

Mass spectrometry

The positive and negative ion modes of each sample were detected via electrospray ionization (ESI). The samples were separated via UPLC and analyzed using the TripleTOF 5600+ Mass Spectrometer (Sciex). The ESI source conditions were as follows: Ion Source Gas1 (Gas1), 60 psi; Ion Source Gas2 (Gas2), 60 psi; curtain gas (CUR), 30 psi; source temperature, 600 °C; IonSapary Voltage Floating (ISVF), $\pm 5,500$ V; time-of-flight (TOF) MS scan m/z range, 60–1,200 Da; product ion scan m/z range, 25–1,200 Da; TOF MS scan accumulation time, 0.15 s/spectra; product ion scan accumulation time, 0.03 s/spectra. Second-stage MS was performed via information-dependent acquisition (IDA) and adopted a high-sensitivity mode: declustering potential (DP), ± 60 V (positive and negative modes); collision energy, 30 eV. The IDA setting was as follows: exclude isotopes within 4 Da; candidate ions to monitor per cycle, 6.

Data pre-processing

After format conversion of the original data, the XCMS program in MS-DIAL software was used for peak alignment, retention time correction, and peak area extraction. The structure of the metabolites was identified via accurate mass number matching (<25 ppm) and secondary spectrum matching, and the public HMDB and MassBank databases were searched.

For the extracted data, ion peaks with missing values >50% in the group were deleted, positive and negative ion peaks were integrated, and pattern recognition was carried out using SIMCA-P14.1 software (Umetrics, Umea, Sweden).

Multidimensional statistical analysis was

performed after pre-processing the data via Pareto scaling (Par), including unsupervised principal component analysis (PCA), supervised partial least square discriminant analysis (PLS-DA), and orthogonal partial least square discriminant analysis (OPLS-DA).

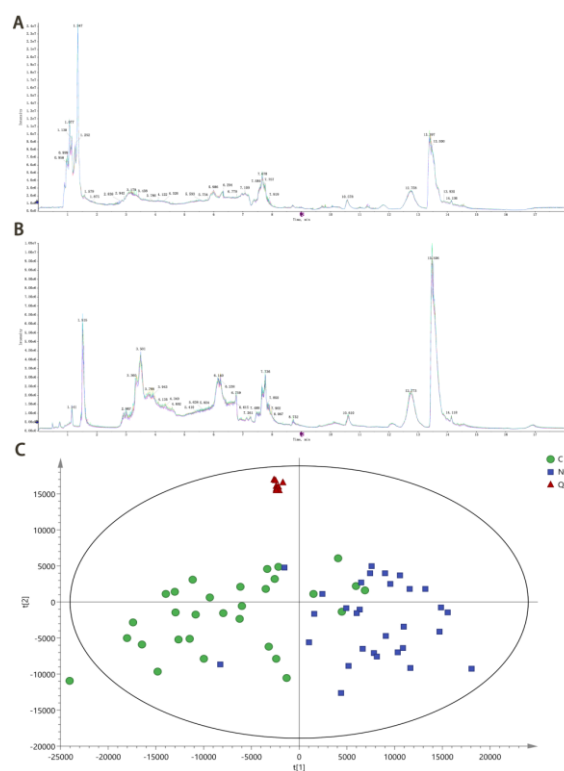
RESULTS

Experimental quality evaluation

Total ion chromatography (TIC) plot comparison of QC sample mass spectra

The TIC values of the QC sample mass spectra obtained in the positive and negative ion detection modes were compared by overlaying the spectra (Fig. 1a, b). The response intensities and peak retention times overlapped, indicating that the variation caused by instrument error was small and the data quality was reliable.

FIGURE 1. Positive (a) and negative (b) ion mode total ion chromatogram profiles for quality control samples. (c) Principal component analysis scores of the samples (t[1] for principal component 1 and t[2] for



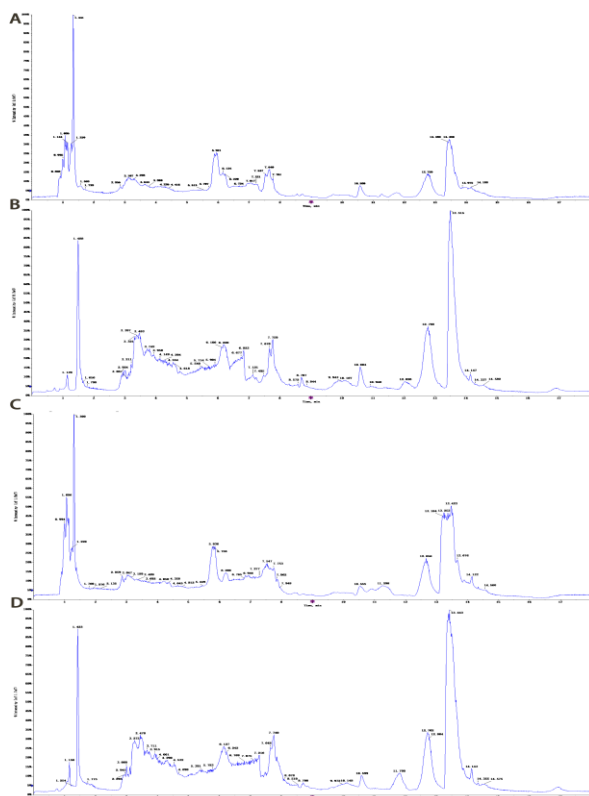
Overall sample PCA

The ion peaks of metabolites were extracted using MS-DIAL software; there were 15,239 ion peaks in the positive ion mode and 9,505 in the negative ion mode. The peaks obtained from all experimental and QC samples were extracted, processed with Par, and subjected to PCA. The PCA model obtained using seven cycles of cross-validation is shown in Fig. 1c. The QC samples were more closely clustered (Fig. 1c), indicating good reproducibility. Overall, the instrumental analysis was stable, implying reliable experimental data. The differences in the metabolic profiles obtained reflect biological differences between the samples.

Sample metabolic MS TIC plots

Each sample was analyzed using UPLC-quadrupole-time-of-flight (Q-TOF) (LC-MS/MS) to obtain two mass spectral raw files (positive and negative ion modes). Figure 2a, b and 2c, d shows the mass spectral TIC plots of group C and NC samples in the positive and negative ion detection modes, respectively.

FIGURE 2. Positive (a) and negative (b) ion mode total ion chromatogram profiles for the papillary thyroid carcinoma samples. Positive (c) and negative (d) ion mode total ion chromatogram profiles for the paracancerous tissue group.



Principal component analysis

Principal component analysis was performed to compare group C and NC samples. The PCA model parameters obtained with seven cycles of cross-validation are shown in Table 1, and the PCA model score plot is shown in Fig. 3a. The overall distribution trend among all samples was observed using PCA, and the score plot of PCA for PC1 (i.e., the first principal component) is shown in Fig. 3b. The intergroup differences between cancer and paracancerous tissue samples were significant in the positive and negative ion modes.

Table 1: PCA model parameters

Sample comparison group	A	R ² X (cum)	Q ² (cum)
QC	9	0.568	0.26
NC vs. C	9	0.564	0.177

A indicates the principal component score, R²X indicates the model explanation rate, and Q² indicates the model's predictive power. NC, paracancerous tissue group; C, papillary thyroid carcinoma group; PCA, principal component analysis.

Partial least square discriminant analysis

The PLS-DA model for each comparison group was developed, and the model evaluation parameters (R²Y, Q²) obtained with 7-fold cross-validation are shown in Table 2. The model scores are plotted in Fig. 3c. If R² and Q² are closer to 1, the model is more stable and reliable; conversely, if R² and Q² are less than 0.5, the model is less reliable. The results showed significant intergroup differences in the metabolomics of cancer and paracancerous tissue samples in the positive and negative ion mode models.

FIGURE 3. (a) Principal component analysis score graph for papillary thyroid carcinoma (PTC) and paracancerous tissues. The green dots represent paracancerous tissue and the blue squares represent PTC tissue. (b) Principal component 1 (PC1) score graph for NC vs. C. (c) Partial least square discriminant analysis scores for NC vs. C. (d) Orthogonal partial least square discriminant analysis score chart for NC vs. C. (e) Orthogonal

partial least square discriminant analysis displacement test for NC vs. C. NC, paracancerous tissue group; C, papillary thyroid carcinoma group.

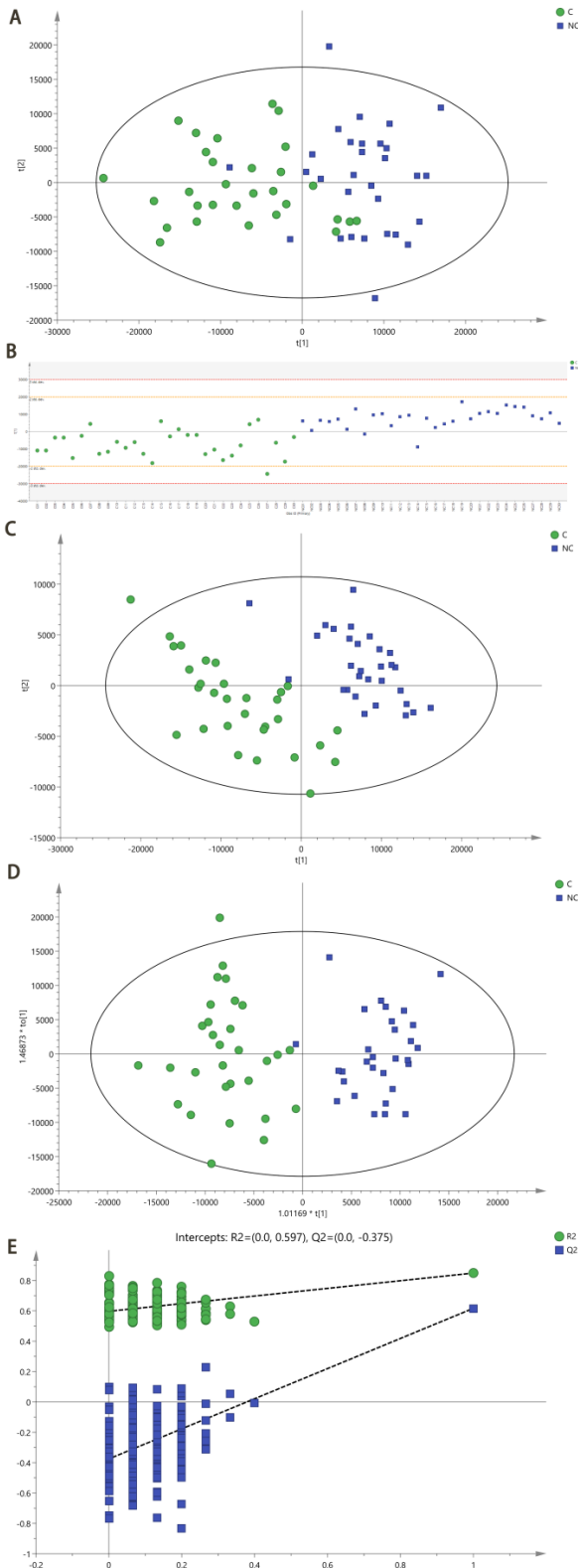
TABLE 2
Evaluation parameters of the PLS-DA model

Sample comparison group	A	R ² X (cum)	R ² Y (cum)	Q ² (cum)
NC vs. C	2	0.215	0.849	0.177

R² indicates the explanatory rate of the model and Q² indicates the predictive power of the model. The closer the R² and Q² are to 1, the more stable and reliable the model. NC, paracancerous tissue group; C, papillary thyroid carcinoma group; PLS-DA, partial least square discriminant analysis.

Orthogonal partial least square discriminant analysis

The variable importance for projection (VIP) was calculated to measure the strength and explanatory power of the expression pattern of each metabolite in the categorical discrimination of each group of samples, thus aiding marker metabolite screening (generally, a VIP score of >1.0 is used as the screening criterion). The OPLS-DA model for each comparison group was established, and the model evaluation parameters (R²Y and Q²) obtained with 7-fold cross-validation are shown in Table 3. R² and Q² values closer to 1 indicate greater model stability and reliability; conversely, R² and Q² values less than 0.5 indicate lower model reliability. The model score plot is shown in Fig. 3d. The OPLS-DA model could clearly distinguish between the groups of samples. The R² and Q² of the OPLS-DA model built from the experimental data were ≥0.5, implying a reliable and stable model. Figure 3e shows a plot of the permutation test based on the OPLS-DA model for this group. The horizontal coordinates of the permutation test represent the correlation between Y of the random group and Y of the original group, and the vertical coordinates represent the R² and Q² values. The Q² intercept was less than 0.05, indicating no overfitting.



A indicates the principal component score, R^2Y indicates the model explanation rate, and Q^2 indicates the predictive power of the model. The closer R^2Y and Q^2 are to 1, the more stable and reliable the model. R^2 and Q^2 intercepts indicate the intercept between R^2 and Q^2 regression. NC, precancerous tissue group; C, papillary thyroid carcinoma group; OPLS-DA, orthogonal partial least square discriminant analysis.

Univariate statistical analysis

Commonly used univariate analysis methods for differentially expressed metabolite analysis between groups of samples include fold-change analysis (FC analysis), t-tests, and volcano plot analysis, which combines the first two methods. The univariate analysis can be used to visualize the significance of metabolite changes between groups and thus help screen for potential marker metabolites (FC > 2 or FC < 0.5 and $P < 0.05$ were used as screening criteria in this study). Figure 4a is a volcano plot for the comparison between groups C and NC. Differentially expressed metabolites were screened using univariate statistical analysis.

FIGURE 4: (a) Differentially expressed metabolites between the papillary thyroid carcinoma and paracancerous thyroid tissue groups. Red dots represent upregulated metabolites and green dots represent downregulated metabolites. (b) Hierarchical clustering of significantly different metabolites in NC vs. C. (c) Heat map of significantly differentially expressed metabolites in the correlation coefficient matrix. The correlation coefficient between metabolites is represented as a colored circle, where $R > 0$ indicates a positive correlation and is represented in red, and $R < 0$ indicates a negative correlation and is represented in blue. Larger circles and darker colors indicate a stronger correlation.

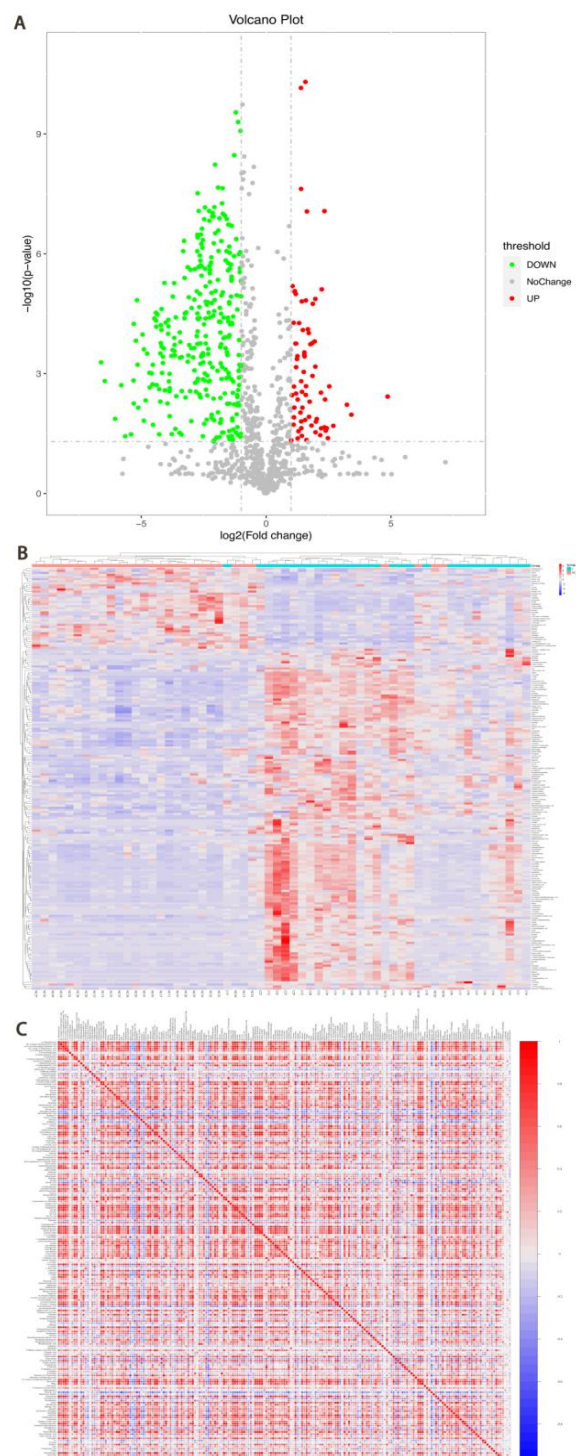


TABLE 3: Evaluation parameters of the OPLS-DA model

Sample comparison group	A	R^2X (cum)	R^2Y (cum)	Q^2 (cum)	R^2 intercept	Q^2 intercept
NC vs. C	1+1+0	0.215	0.849	0.616	0.597	-3.75

TABLE 4 Differentially expressed metabolites in papillary thyroid carcinoma and paracancerous tissues in positive and negative ion modes (Top 15, FC < 0.5)

No.	Metabolite	VIP	FC (NC/C)	P
1	L-Norvaline	6.8423	0.0278	0
2	Bisphenol S	5.8236	0.4597	0
3	Leucine	5.7582	0.308	0
4	(S)-3-Amino-4-phenylbutyric acid	5.4321	0.1487	0
5	Isoleucylisoleucine	4.5075	0.2671	0
6	Gly-Leu	4.0201	0.1637	0
7	L-Valine	3.8381	0.2632	0
8	Alanine	3.6419	0.0779	0
9	Nerolidol	3.5595	0.0961	0.0004
10	Tryptophan	3.1445	0.1321	0.0004
11	(Z)-2-Octylpent-2-enedioic acid	3.0889	0.4104	0
12	Propoxyphene	3.0839	0.2712	0.0001
13	Methionine	2.8601	0.308	0.0001
14	Trans-cinnamic acid	2.729	0.2186	0
15	L-Beta-homothreonine	2.6063	0.0474	0.0001

VIP, variable projection importance; FC, fold-change. NC, paracancerous tissue group; C, papillary thyroid carcinoma group.

TABLE 5: Differentially expressed metabolites in papillary thyroid carcinoma and paracancerous tissues in positive and negative ion modes (Top 15, FC > 2)

No.	Metabolite	VIP	FC (NC/C)	P
1	Dibucaine	1.3518	5.2285	0.0268
2	Propyzamide	2.2084	5.0516	0
3	Tyrosine	2.1861	3.9229	0.0007
4	Pidotimod	5.057	3.6022	0.0002
5	Deoxysappanone B 7,4'-dimethyl ether	1.9435	3.0312	0.0021
6	Hippurate	1.5693	3.0166	0
7	Emodic Acid	1.47	2.9797	0
8	Perseitol	1.1308	2.9123	0.0004
9	Nitrendipin	1.2662	2.8878	0.0003
10	2,6-Dimethoxyquinone	1.0622	2.7386	0.0071
11	L-Thyroxine	1.4033	2.6938	0.0361
12	Dysidin	1.0193	2.6923	0
13	Beta-indoleacetic acid	1.4043	2.6316	0
14	Fenuron	1.6225	2.4033	0.0044
15	3-Methylxanthine	1.5715	2.3601	0.0004

VIP, variable projection importance; FC, fold-change. NC, paracancerous tissue group; C, papillary thyroid carcinoma group

Significantly differentially expressed metabolite levels

The VIP values obtained from the OPLS-DA model were used to measure the intensity and explanatory power of the expression pattern of each metabolite in the discrimination of each group of samples and to mine for biologically significant differentially expressed metabolites (Table 3). In the positive and negative ion modes, the conditions of $VIP > 1.0$, $P < 0.05$, $FC > 2.0$, and $FC < 0.5$ were combined to yield a total of 152 differentially expressed metabolites in cancer and paraneoplastic tissues (including 23 with $FC > 2.0$ and 129 with $FC < 0.5$). The details of the top 15 differentially expressed metabolites sorted by VIP values are listed in Tables 4 and 5.

Bioinformatic analysis Hierarchical cluster analysis

To evaluate the candidate metabolites and comprehensively visualize the relationships between samples and the differences in metabolite expression patterns among samples, we used qualitative hierarchical clustering of qualitatively significantly differentially expressed metabolites for each group of samples. This analysis enabled us to accurately screen for marker metabolites and examine the associated metabolic processes. Generally, when the candidate metabolites are reasonably accurate, the same group of samples cluster together. At the same time, metabolites in the same cluster have similar expression patterns and are likely to be in close proximity to each other in the metabolic process. Figure 4b shows the hierarchical clustering results of significantly differentially expressed metabolites for the comparison between groups C and NC.

Correlation coefficient matrix

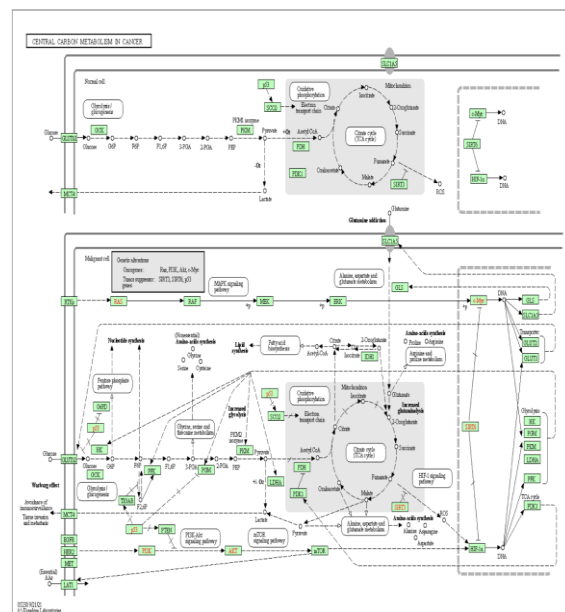
Correlation coefficients between significantly differentially expressed metabolites were calculated using Pearson correlation analysis. The correlations between significantly differentially expressed metabolites are presented as a heat map of the correlation coefficient matrix of NC vs. C (Fig. 4c). This matrix shows the correlation between significantly differentially expressed metabolites.

Kyoto Encyclopedia of Genes and Genomes (KEGG) metabolic pathway analysis

Figure 5 shows a map of the cancer carbon metabolic pathways associated with the significantly

differentially expressed metabolites in NC vs. C. The results showed that three transcription factors, C-myc, HIF-1, and p53, are key regulators of tumor metabolism and coordinate tumor metabolism differentially, with many other oncogenes clustering along signaling pathways regulating c-myc, HIF-1, and p53 expression.

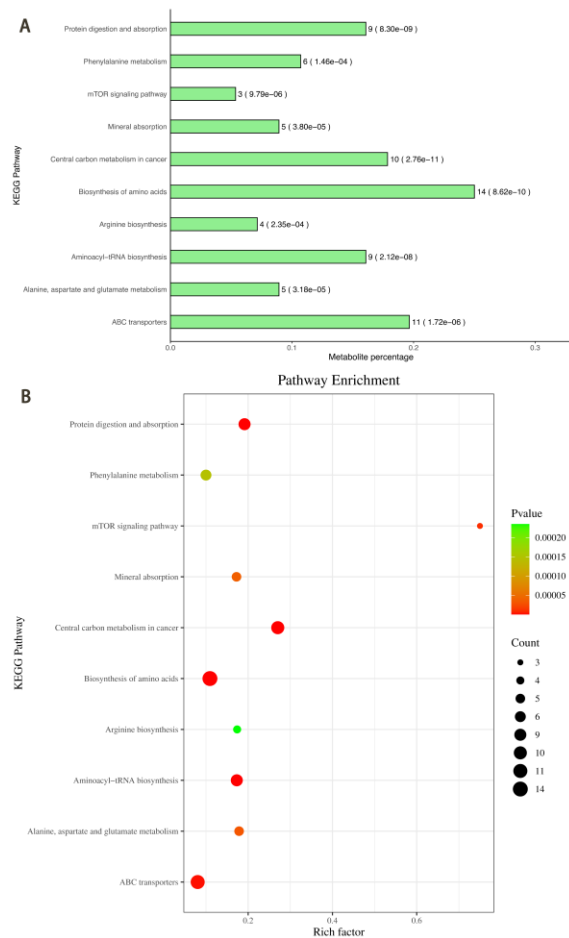
Figure 5: Map of the cancer carbon metabolic pathways associated with the significantly differentially expressed metabolites in the papillary thyroid carcinoma and paracancerous tissue groups



Kyoto Encyclopedia of Genes and Genomes pathway enrichment analysis

The significantly differentially expressed metabolites obtained from the comparison groups were subjected to KEGG metabolic pathway enrichment analysis (Fig. 6a, b). The significantly differentially expressed metabolites are mainly involved in protein digestion and absorption; phenylalanine metabolism; mammalian target of rapamycin (mTOR) signaling pathway; mineral uptake; cancer carbon metabolism; amino acid biosynthesis; arginine biosynthesis; aminoacyl-tRNA biosynthesis; alanine, aspartate, and glutamate metabolism; ABC transport; and other metabolic pathways.

FIGURE 6. (a) Kyoto Encyclopedia of Genes and Genomes (KEGG) metabolic pathway enrichment analysis of the significantly differentially expressed metabolites of NC vs. C (Top 10). (b) Kyoto Encyclopedia of Genes and Genomes metabolic factor enrichment analysis of the significantly differentially expressed metabolites of NC vs. C (Top 10)



DISCUSSIONS

Here, UPLC-Q-TOF LC-MS liquid MS was used to analyze the overall metabolite changes between PTC and matched paraneoplastic tissues. Control experiments showed that the instrumental analysis used was stable, and the experimental data were stable and reliable; therefore, the differences in the metabolic profiles obtained in this study reflect the biological differences between the samples. The OPLS-DA identified 152 differentially expressed metabolites, and KEGG pathway enrichment analysis showed that the differentially expressed metabolites in PTC and

paraneoplastic tissue are mainly associated with the metabolism and biosynthesis of amino acids and the mTOR signaling pathway. According to the OPLS-DA results, the levels of metabolites such as dibucaine, proprizamide, tyrosine, pidotimod, deoxysappanone B 7,4'-dimethyl ether (Deox B 7,4), hippurate, and emodic acid were significantly elevated in PTC. Tyrosine phosphorylation is a broad post-translational modification essential for promoting metabolic reprogramming in cancer cells,²² and multiple cancer types exhibit "oncogenic addiction" to receptor tyrosine kinase dysregulation.^{17,27} showed that pidotimod enhanced the antitumor effects of cisplatin in mouse lung cancer by promoting the infiltration of dendritic and CD8T+ cells and upregulating the expression of IFN- γ and granzyme B. The antitumor effects of cisplatin in mouse lung cancer were enhanced by the expression of IFN- γ and granzyme B. Deox B 7,4 potentially inhibits the antitumor effects of cisplatin in mouse lung cancer by inhibiting the Slit2/Robo1/2, SLIT3/Robo4, COX2/PTP-Rb/pik3r2, and DLL4/hey2/efnb2a signaling pathways and VEGFR-2/FGFR1/MMP9 activation to exert anti-angiogenic effects.² However, the link among dibucaine—whose level is most significantly elevated in PTC—proprizamide, and thyroid cancer, has not been reported.

According to the OPLS-DA results, the levels of metabolites such as L-norvaline, bisphenol S, leucine, (S)-3-amino-4-phenylbutyric acid, isoleucylisoleucine, gly-leu, and L-valine were significantly reduced in PTC.¹⁵ reported that L-norvaline treatment reversed cognitive decline in mice with Alzheimer's disease. This treatment was neuroprotective, and it reduced β -amyloid degeneration, attenuated microglial proliferation, and decreased tumor necrosis factor transcript levels.²⁹ showed that the spatial distribution of ceramide-sphingomyelin signaling pathway-related lipids and chromosomal stability-related proteins, and cell proliferation were altered in the central necrotic zone of breast tumors following bisphenol S-10 (BPS-10; 10 μ g/kg body weight/day) exposure, with a more pronounced

proliferation of breast tumor cells. In contrast, BPS-100 exposure significantly accelerates breast tumor progression due to changes in the spatial distribution of proteins associated with nucleic acid structural stability in the surrounding tumor region. Intracellular leucine regulates cell growth by binding to sestrin2, a negative regulator of mTOR complex 1 (mTORC1), disrupting the link between sestrin2 and gator2, a positive regulator of mTORC1 activity.^{25,26} Additionally, acetyl coenzyme A positively regulates mTORC1 activity through EP300-mediated acetylation of mTORC1 regulator raptor at K1097.²⁵ Thus, leucine plays a central role in amino acid sensing by mTORC1, and the mTORC1 signaling pathway can also influence lipid and nucleotide syntheses, serving as a link between amino acid sensing and other anabolic processes.¹ Nerolidol inhibits the proliferation of uterine leiomyoma cells through reactive oxygen species-induced DNA damage and downregulation of the ATM/Akt pathway.⁵ No link between (S)-3-amino-4-phenylbutyric acid or isoleucylisoleucine and thyroid cancer has been reported, and further studies are required to confirm this.

The KEGG pathway enrichment analysis showed that the differentially expressed metabolites in PTC and paraneoplastic tissue are related to amino acid metabolism and biosynthesis and the mTOR signaling pathway. An adequate supply of amino acids is important for cancer cells to maintain their proliferation. In addition to their direct role as substrates for protein synthesis, they may play a role in producing energy, driving nucleoside synthesis, and maintaining cellular redox homeostasis. Studies on amino acid metabolism in cancer have highlighted a delicate network, and in many cases, tracking the uptake and use of specific amino acids may not reveal the actual function of a pathway.²³ Mammalian target of rapamycin, a highly conserved serine/threonine protein kinase, exists as mammalian target of rapamycin complex 1 (mTORC1) and 2 (mTORC2).⁸ Mammalian target of rapamycin complex 1 includes mTOR, raptor, PRAS40, deptor, mLST8, TEL2, and Tti1. It plays an important activation role in the presence of growth factors and amino acids, depending on the energy status, stress, and oxygen levels, and regulates several biological processes, including lipid metabolism, autophagy, protein

synthesis, and ribosome biogenesis.

Mammalian target of rapamycin complex 2 consists of mTOR, mSin1, rictor, protor, deptor, mLST8, TEL2, and Tti1 and responds to growth factors that control cytoskeleton organization, metabolism, and survival.^{4,7,19,18} Studies have shown that the activation of the PI3K/Akt/mTOR pathway is important in PTC pathogenesis,¹³ consistent with our KEGG pathway enrichment analysis results. Aberrant PTEN methylation patterns have been observed in follicular thyroid cancer and hypo-differentiated or interstitial thyroid cancer, leading to the inactivation of the gene. Methylation of PTEN usually occurs in conjunction with other activating mutations in the PI3K/Akt pathway.^{20,30} Furthermore, germline mutations in PTEN lead to an increased risk of malignancy in several organs, including the thyroid.⁹ Therefore, it has been suggested that PI3K/Akt signaling pathway activation leads to increased PTEN methylation, resulting in reduced PTEN activity, in turn causing further upregulation of the PI3K/Akt pathway.¹³ Thus, further exploration of the effects of kinase inhibitors targeting different members of the PI3K/Akt/mTOR pathway, alone or in combination with other targeted or conventional therapies, may help develop new therapeutic strategies for patients with PTC.

Metabolomic results showed that the levels of amino acids and their derivatives (L- α -amino acids; leucine and its derivatives; β -amino acids and their derivatives; polypeptides; valine and its derivatives; alanine and its derivatives; and methionine and its derivatives) were significantly decreased in PTC. Whereas, the KEGG enrichment analysis showed that the metabolites with significant differences, dibucaine, proprizamide, tyrosine, and pidotimod, were mainly involved in amino acid biosynthesis and metabolism and the mTOR metabolic pathway. Targeting this pathway may represent a novel approach to the treatment of PTC.

Acknowledgment

This work was supported by the Gansu Provincial Science and Technology Program Grant (Natural Science Foundation of Gansu Province), Project No: 22JR5RA646.

Funding Statement

This work was supported by the Gansu Provincial Science and Technology Program Grant (Natural Science Foundation of Gansu Province), Project No: 22JR5RA646.

Competing interests

The authors declare no conflicts of interest.

Author Contributions

All authors contributed to the study's conception and design. Material preparation was performed by Guodong Man and Jianli Wang. Data collection and analysis were performed by Guodong Man, Juan Wang, Qinjiang Liu, Jun Wang, and Jianye Zhou. The first draft of the manuscript was written by Ruixia Ma, and all authors commented on previous versions of the manuscript. All authors read and approved the final manuscript.

Availability of Data and Materials

The data that support the findings of this study are available from the corresponding author on reasonable request.

Ethics Approval

The ethics committee of the Gansu Provincial People's Hospital approved this study (approval number: P202205300031).

Consent to Participate

Informed consent was obtained from all individual participants included in the study.

Consent to Publish

The authors affirm that human research participants provided informed consent for the publication of the images in Figures 1–6.

Conflict of Interest

The authors declare that they have no conflicts of interest to report regarding the present study.

References

1. Ben-Sahra I, Manning BD. mTORC1 signaling and the metabolic control of cell growth. *Curr Opin Cell Biol* 2017;45:72–82.
2. Chen K, Fan Y, Gu J, et al. In vivo screening of natural products against angiogenesis and mechanisms of anti-angiogenic activity of deoxysappanone B 7,4'-dimethyl ether. *Drug Des Devel Ther* 2020;14:3069–3078.
3. Clement SC, Kremer LCM, Links TP et al. Is outcome of differentiated thyroid carcinoma influenced by tumor stage at diagnosis? *Cancer Treat Rev* 2015;41:9–16.
4. Dibble CC, Manning BD. Signal integration by mTORC1 coordinates nutrient input with biosynthetic output. *Nat Cell Biol* 2013;15:555–564.
5. Dong JR, Chang WW, Chen SM. Nerolidol inhibits proliferation of leiomyoma cells via reactive oxygen species-induced DNA damage and downregulation of the ATM/Akt pathway. *Phytochemistry* 2021;191:112901.
6. Huang J, Ngai CH, Deng Y, et al. Incidence and mortality of thyroid cancer in 50 countries: a joinpoint regression analysis of global trends. *Endocrine* 2023;80:355–365.
7. Huang K, Fingar DC. Growing knowledge of the mTOR signaling network. *Semin Cell Dev Biol* 2014;36:79–90.
8. Kennedy BK, Lamming DW. The mechanistic target of rapamycin: the grand Conductor of metabolism and aging. *Cell Metab* 2016;23:990–1003.
9. Liaw D, Marsh DJ, Li J, et al. Germline mutations of the PTEN gene in Cowden disease, an inherited breast and thyroid cancer syndrome. *Nat Genet* 1997;16:64–67.
10. Lim H, Devesa SS, Sosa JA, et al. Trends in thyroid cancer incidence and mortality in the United States, 1974–2013. *JAMA* 2017;317:1338–1348.
11. Nicholson JK, Lindon JC, Holmes E. 'Metabonomics': understanding the metabolic responses of living systems to pathophysiological stimuli via multivariate statistical analysis of biological NMR spectroscopic data. *Xenobiotica* 1999;29:1181–1189.
12. Patti GJ, Yanes O, Siuzdak G. Innovation: Metabolomics: the apogee of the omics trilogy. *Nat Rev Mol Cell Biol* 2012;13:263–269.
13. Petrulea MS, Plantinga TS, Smit JW, et al. PI3K/Akt/mTOR: a promising therapeutic target for non-medullary thyroid carcinoma. *Cancer Treat Rev* 2015;41:707–713.
14. Plumb RS, Granger JH, Stumpf CL, et al. A rapid screening approach to metabonomics using UPLC and oa-TOF mass spectrometry: application to age, gender and diurnal variation in normal/Zucker obese rats and black, white and nude mice. *Analyst* 2005;130:844–849.
15. Norvaline, a new therapeutic agent against Alzheimer's disease. *Neural Regen Res* 2019;14:1562–1572.
16. cancer incidence and deaths to 2030: the unexpected burden of thyroid, liver, and pancreas cancers in the United States. *Cancer Res* 2014;74:2913–2921.
17. Saraon P, Pathmanathan S, Snider J, et al. Receptor tyrosine kinases and cancer: oncogenic mechanisms and therapeutic approaches. *Oncogene* 2021;40:4079–4093.
18. Saxton RA, Sabatini DM. mTOR signaling in growth, metabolism, and disease. *Cell* 2017;68:960–976.
19. Shimobayashi M, Hall MN. Making new contacts: the mTOR network in metabolism and signalling crosstalk. *Nat Rev Mol Cell Biol* 2014;15:155–162.

20. Soria JC, Lee HY, Lee JI, et al. Lack of PTEN expression in non-small cell lung cancer could be related to promoter methylation. *Clin Cancer Res* 2002;8:1178–1184.
21. Sung H, Ferlay J, Siegel RL, et al. Global cancer statistics 2020: GLOBOCAN estimates of incidence and mortality worldwide for 36 cancers in 185 countries. *CA Cancer J Clin* 2021;71:209–249.
22. Taddei ML, Pardella E, Pranzini E, et al. Role of tyrosine phosphorylation in modulating cancer cell metabolism. *Biochim Biophys Acta Rev Cancer* 2020;1874:188442.
23. Vettore L, Westbrook RL, Tennant DA. New aspects of amino acid metabolism in cancer. *Br J Cancer* 2020;122:150–156.
24. Wishart DS. Is cancer a genetic disease or a metabolic disease? *EBioMedicine* 2015;2:478–479.
25. Wolfson RL, Chantranupong L, Saxton RA, et al. Sestrin2 is a leucine sensor for the mTORC1 pathway. *Science* 2016;351:43–48.
26. Wolfson RL, Sabatini DM. The dawn of the age of amino acid sensors for the mTORC1 pathway. *Cell Metab* 2017;26:301–309.
27. Wu T, Cui J, Gao J, et al. Pidotimod enhanced the anti-growth effect of cisplatin on lung cancer in mice via promoting antitumor immune response. *Biochem Biophys Res Commun* 2020;528:678–684.
28. Zhang S, Niu L. Evaluation of the efficacy and the limitation of ultrasound-guided core-needle biopsy, core-needle aspiration and fine-needle aspiration in micro-nodules of thyroid. *Zhonghua Er Bi Yan Hou Tou Jing Wai Ke Za Zhi* 2014;49:893–896.
29. Zhao C, Yong T, Zhang Y, et al. Breast cancer proliferation and deterioration-associated metabolic heterogeneity changes induced by exposure of bisphenol S, a widespread replacement of bisphenol A. *J Hazard Mater* 2021;414:125391.
30. Zysman MA, Chapman WB, Bapat B. Considerations when analysing the methylation status of PTEN tumor suppressor gene. *Am J Pathol* 2002;160:795–800.